Numerical Computation of Turbulent Gas-Solid Particle Flow in a 90° Bend

J. Y. Tu and C. A. J. Fletcher
Centre for Advanced Numerical Computation in Engineering and Science (CANCES),
The University of New South Wales, Sydney 2052, Australia

A numerical computation of the LDV results of Kliafas and Holt is reported for a turbulent gas–solid particle flow in a square-sectioned 90° bend. A Eulerian model with generalized Eulerian solid surface boundary conditions for the particulate phase is employed. In the momentum balance equation, the particulate-phase momentum exchanges with solid walls are included. The turbulent closure is effected by using the gas-phase RNG-based k-ϵ turbulence model, and the particulate turbulence diffusivity is related to the turbulent viscosity of the gas phase. Comparisons are made with experimental data for the mean streamwise velocities of both phases, the streamwise turbulence intensity of the gas phase, and the particulate concentration distribution in the bend. The localized high particulate concentration near the outer curve of the bend that occurs at large Stokes number is accurately predicted. Empirical computational evidence is presented for a relaxation of the minimum particle number density required to allow the use of a continuum model.

Introduction

The erosion of material by solid particle impact is a serious problem in coal combustion equipment, coal liquefaction–gasification pipeline systems, and many chemical plants. For coal gasification systems the problem of erosive wear is quite severe at pipe bends. The successful design and determination of optimum operating conditions of such systems requires measurement, analysis, and prediction of the hydrodynamics of the the turbulent gas–solid particle (two-phase) flows in the components composing the system. Due to the complexity of the fundamental processes governing particle motion, to explain the complicated phenomena present in gas–particle two-phase flows is also of considerable academic interest.

Kliafas and Holt (1987) have made detailed measurements of a turbulent gas–solid particle flow, using a laser Doppler velocimetry (LDV) technique, in a square-sectioned (10×10 cm) 90° vertical to horizontal bend with a bend radius equal to 1.76 times the hydraulic diameter of the duct. Two bulk velocities of 33.09 and 52.19 m/s corresponding to two different Reynolds numbers, 2.2×10^5 and 3.47×10^5, were employed. Glass spheres 50 and 100 μm in diameter were used to represent the solid particle phase. The experiment was restricted to a very dilute suspension (the volumetric ratios were less than 10^{-7}) so that the gas flow field is negligibly affected by the presence of particles. The mean velocities and turbulence intensity profiles of both the gas and solid phases at the symmetry plane of the duct were provided. The particle distributions along the centerline at different cross sections of the bend were also measured for the particle size of 50 μm in diameter. The particulate velocity profiles were found to be quite flat across the transverse section. The particles were mainly concentrated in the outer wall region after the flow passed through about half of the bend. The experiment was designed to provide the data necessary to assist in improving numerical models for dilute turbulent gas–solid particle flows. However, no numerical prediction that can be compared with the experimental data just mentioned has been previously carried out.

The present article reports a computational comparison and analysis of the LDV results of Kliafas and Holt (1987) for a turbulent gas–solid particle flow in a 90° bend with a square cross section, using a two-fluid model (Eulerian approach) developed by Tu and Fletcher (1994). The formulation of the governing equations for the dispersed particulate phase used in our model follows that of Adeniji-Fashola and Chen (1990), which is based on the model developed by Chen and Wood (1985). However, a set of generalized Eulerian

solid surface boundary conditions for solving the governing equations of the particulate phase and a particle-wall collision model are included in the model. This is particularly important for the near-wall region, which is a key feature of the Kliafas and Holt experiments. The renormalization group (RNG) based k-ϵ turbulence model is used in this article for taking the turbulence effects into account instead of using the standard k-ϵ turbulence model.

It is worthwhile noting that this type of formulation of governing equations for the particulate phase is used in a number of engineering calculations (Chen and Wood, 1986; Pourahmadi and Humphrey, 1983; Rizk and Elghobashi, 1989). Recent analyses (Reeks, 1992, 1993) and simulation (Simonin et al., 1994) for a model problem, Couette flow, suggest that the turbulence modeling may be simplified if Favre (mass-weighted) averaging is used instead of Reynolds averaging, and that the use of an isotropic eddy viscosity for the particulate phase may not be appropriate for certain classes of low-loading flow at intermediate Stokes number. The current status of turbulence modeling for the particulate phase is reviewed by Elghobashi (1994). For the current problem, typical Stokes numbers are larger and the turbulence modeling is not expected to be a critical factor. In addition, special care is required in using a mass weighted averaging approach to account for the fluctuations of the momentum transfer term in the averaging process requiring separate contributions, due to the drag, fluid pressure, and added mass force fluctuations, in terms of the fluid–particle velocity correlations (Gosman et al., 1992; Issa and Oliveira, 1994).

The current interest is to predict the gas–solid two phase flow in a complex geometry by implementing the developed particle-wall collision model and the Eulerian wall boundary conditions into the two-fluid model. The focus will be on the comparison of the mean streamwise velocities of both the gas and solid particle flow through the 90° bend with a square cross section, with the experimental data of Kliafas and Holt (1987). Because Kliafas and Holt used a very dilute particle suspension, the question of whether the continuum assumption in the Eulerian model is still valid is also addressed in this article. The comparison of mean streamwise velocity profiles of both the gas and particulate phases indicates very satisfactory agreement with experimental data. For the particulate concentration, a remarkable qualitative agreement of the predicted distribution with the measured data is obtained in the present work.

Governing Equations

In an Eulerian model, both gas and particulate phases are considered as a continuum and a set of Reynolds-averaged conservation equations for the mass and momentum of both phases, gas kinetic energy of turbulence, and its dissipation can be written in a generic transport form (Fletcher, 1993; Tu and Fletcher, 1994)

$$\frac{\partial}{\partial x_i}(A_i\phi) - \frac{\partial}{\partial x_i}\left(B\frac{\partial \phi}{\partial x_i}\right) = S. \tag{1}$$

Gas phase

Continuity equation ($\phi = 1$)

$$A_i = \rho_g u_g^i; \qquad B = 0; \qquad S = 0. \tag{2}$$

Momentum equation ($\phi = u_g^i$)

$$A_i = \rho_g u_g^i; \qquad B = \mu_{g,\text{eff}}; \qquad S = -\frac{\partial P}{\partial x_i}. \tag{3}$$

Turbulent kinetic energy equation ($\phi = k$)

$$A_i = \rho_g u_g^i; \quad B = \alpha\mu_{gt}; \qquad S = P_k - \rho_g\epsilon. \tag{4}$$

ϵ-equation ($\phi = \epsilon$)

$$A_i = \rho_g u_g^i; \qquad B = \alpha\mu_{gt}; \qquad S = \frac{\epsilon}{k}(C_{\epsilon 1}P_k - C_{\epsilon 2}\rho_g\epsilon) - R. \tag{5}$$

Particulate phase

Continuity equation ($\phi = \rho_p$)

$$A_i = \rho_p u_p^i; \qquad B = \rho_p D_p; \qquad S = \left[\rho_p u_p^i - D_p\frac{\partial \rho_p}{\partial x_i}\right]\frac{\partial \rho_p}{\partial x_i}. \tag{6}$$

Momentum equation ($\phi = u_p^i$)

$$A_i = \rho_p u_p^i; \qquad B = \rho_p \nu_p; \qquad S = \frac{\partial}{\partial x_i}\left(\rho_p\nu_p\frac{\partial u_p^i}{\partial x_k}\right) + \frac{\partial}{\partial x_i}\left[D_p\left(u_p^i\frac{\partial \rho_p}{\partial x_k} + u_p^k\frac{\partial \rho_p}{\partial x_i}\right)\right] + F_D + F_G + F_{WM}. \tag{7}$$

In the preceding governing equations, it is assumed that since the particulate phase is dilute, interparticle collision is negligible and the particulate behavior has no influence on the gas flow solution. The second-order turbulence correlation terms due to the averaging process have been modeled using a gradient hypothesis (Chen and Wood, 1985; Adeniji-Fashola and Chen, 1990)

$$-\overline{\rho_p' u_p''} = D_p\frac{\partial \rho_p}{\partial x_i}$$

$$-\rho_p\overline{u_p'' u_p''} = \mu_p\left(\frac{\partial u_p^i}{\partial x_j} + \frac{\partial u_p^j}{\partial x_i}\right), \tag{8}$$

where the particulate turbulent diffusivities D_p and μ_p are related to the turbulent viscosity of the gas phase ν_{gt} by Adeniji-Fashola and Chen (1990)

$$D_p = \frac{\nu_p}{S_c}; \qquad \nu_p = \frac{\mu_p}{\rho_p} = K_p \nu_{gt} \tag{9}$$

and S_c is the turbulent Schmidt number taken to be 0.7; K_p is a weight factor accounting for the particle inertia, which is given by

$$K_p = \max[K_d, 1/(1+S_t^t)], \tag{10}$$

where K_d is a numerical dissipation and S_t^t is the turbulent Stokes number, $= t_p/t_e$. Here t_p is a particle response or relaxation time, $t_p = \rho_s d_p^2/18\mu_g$, where ρ_s is the material density of particles and d_p the diameter of the particle. The eddy characteristic time follows the work of Adeniji-Fashola and Chen (1990) for the confined two-phase flow, $t_e = 0.125k/\epsilon$. Thus, K_p is reflecting the transfer of turbulence energy to the particulate phase due to the particle inertia. The typical magnitude of $1/(1+S_t^t)$ for the present case is between 0.2 and 0.01. In some regions, particularly near the wall, this value gets very small (less than 0.001) so that K_d is taken to be 0.01 to avoid numerical instability. The choice of different coefficients in the formula for the time scale of turbulence, t_e, such as used in Chen and Wood (1985) or Adeniji-Fashola and Chen (1990) is insensitive because of the high particle inertia in the present case.

One difference between the current formulation and the previous ones, such as one of Adeniji-Fashola and Chen (1990), is that a recently developed turbulence model, the dynamic renormalization group theory (RNG) based k-ϵ turbulence model (Yakhot and Orszag, 1986), is employed in this study. In the RNG turbulence transport equation, an inverse Prandtl number α is introduced and can be obtained from the following equation:

$$\left|\frac{\alpha - 1.3929}{\alpha_0 - 1.3929}\right|^{0.6321} \left|\frac{\alpha + 2.3929}{\alpha_0 + 2.3929}\right|^{0.3679} = \frac{\nu_1}{\nu_{g,\text{eff}}}, \tag{11}$$

where $\alpha_0 = 1$. The turbulent viscosity ν_{gt} is calculated by $(\nu_{g,\text{eff}} - \nu_1)$, where ν_1 is the laminar viscosity and the effective viscosity $\nu_{g,\text{eff}}$ is computed by

$$\nu_{g,\text{eff}} = \nu_1 \left(1 + \sqrt{\frac{C_\mu}{\nu_1}}\,\frac{k}{\sqrt{\epsilon}}\right)^2. \tag{12}$$

The rate of strain term R in the ϵ-equation is expressed as

$$R = \frac{C_\mu \eta^3 (1 - \eta/\eta_0)}{1 + \beta\eta^3}\,\frac{\epsilon^2}{k}$$

$$\text{and} \qquad \eta = \frac{k}{\epsilon}\left(\frac{\partial u_g^i}{\partial x_j}\left(\frac{\partial u_g^i}{\partial x_j} + \frac{\partial u_g^j}{\partial x_i}\right)\right)^{1/2}, \tag{13}$$

where $\beta = 0.015$, $\eta_0 = 4.38$. According to the RNG theory, the constants in the turbulence transport equations are given to be $C_\mu = 0.0837$, $C_{\epsilon 1} = 1.42$, and $C_{\epsilon 2} = 1.68$, respectively.

For a dilute suspension, the viscous and pressure terms in the particulate phase momentum equations are neglected, but a particle–wall momentum exchange in terms of a momentum source term F_{WM} is included to model the particle–wall interactions in this study. The momentum exchange source term is given by Tu and Fletcher (1994):

$$F_{WM}^N = -C_N\left[1 + \left(\bar{e}_p^N\right)^2\right] \rho_p \left|W_{p,h}^N\right| W_{p,h}^N (B^N)^2 A_n \tag{14}$$

in the normal direction and

$$F_{WM}^T = -C_T\left[1 - \left(\bar{e}_p^T\right)^2\right] \rho_p \left|W_{p,h}^T\right| W_{p,h}^T (B^T)^2 A_n \tag{15}$$

in the tangential direction. Here, A_n denotes a face area of the control volume coincident with the wall; $\bar{e}_p^N$ and $\bar{e}_p^T$ are normal and tangential mean restitution coefficients, respectively; $W_{p,h}^N$ and $W_{p,h}^T$ are normal and tangential mean velocities of particulate phase at the distance h away from the wall; B^N and B^T are constants related to the restitution coefficients; C_N and C_T are coefficients that are modeled by

$$C_N = C_m \frac{W_{p,h}^N}{\left[\sum_{i=1}^{3} \left(u_{p,h}^i\right)^2\right]^{1/2}}, \tag{16}$$

where C_m is referred to as the particle inertial impacting efficiency, which is similar to that obtained by Ilias and Douglas (1989) based on the particle inertia (Stokes number S_t) and the Reynolds number of the gas phase. Referring to the work of Ilias and Douglas, for the present case $C_m = 0.9$ is chosen.

The coefficient C_T is related to the tangential-wall–momentum exchange, which is modeled as

$$C_T = \frac{C_N}{y^+} \qquad \text{for} \qquad y^+ \le 11.63$$

$$C_T = \frac{C_N \kappa}{\ln(Ey^+)} \qquad \text{for} \qquad y^+ > 11.63, \tag{17}$$

where κ and E are the same as in the turbulence model of gas phase (Launder and Spalding, 1974), and y^+ is a similar definition but for the particulate flow (Soo, 1984). Alternatively, the tangential coefficient C_T can be modeled by relating it to the wall friction (Sommerfeld, 1992). The effect of both the normal and tangential-wall–momentum exchanges on the particulate flow is only considered for control volumes immediately adjacent to the wall.

The gravity force is $F_G = \rho_p g$, where g is the gravitational acceleration. The drag force F_D is defined by

$$F_D^i = \rho_p \frac{f\left(u_g^i - u_p^i\right)}{t_p} \tag{18}$$

where the correction factor f is selected according to the work of Schuh et al. (1989).

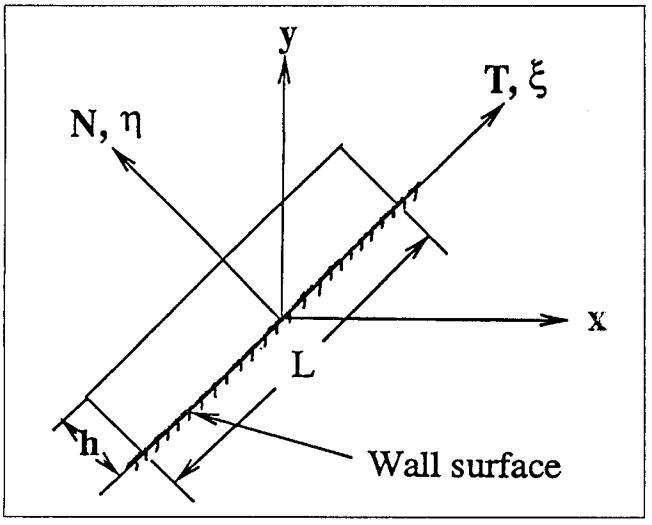

Figure 1. Finite control volume adjacent to a solid wall for deriving wall boundary conditions of particulate phase.

Boundary Conditions

The boundary conditions at inlet are specified for all dependent variables in both the gas and particulate phases. At outflow and symmetry plane the normal gradient of these quantities is set to zero. A "no-slip" boundary condition is employed for the gas velocity at the wall surface. The boundary conditions for the particulate phase at the solid wall are presented in the following, and more details about assumptions and derivations can be found in Tu and Fletcher (1994).

In order to derive the Eulerian formulation of boundary conditions for the particulate phase, we consider a finite control volume adjacent to the surface of a solid wall, as shown in Figure 1. Following a similar strategy to that of the Lagrangian formulation, the mean rebounding characteristics of particles can be expressed approximately by the mean restitution coefficients ($\bar{e}_p^N$ and $\bar{e}_p^T$) and average velocities with Lagrangian components (incident and reflected parts)

$$\overline{W}_{pr,h}^{N,L} = -\bar{e}_p^N \overline{W}_{pi,h}^{N,L} \tag{19a}$$

$$\overline{W}_{pr,h}^{T,L} = \bar{e}_p^T \overline{W}_{pi,h}^{T,L}, \tag{19b}$$

where the superscripts N and T denote the normal and tangential directions; the subscripts i and r refer to the incident and reflected components; h is the distance of control volume top surface away from the wall.

Assuming all incident and reflected particles through the top surface of the control volume, we can impose mass conservation for steady flow

$$N_{pi} \mid \overline{W}_{pi,h}^{N,L} \mid - N_{pr} \mid \overline{W}_{pr,h}^{N,L} \mid = 0 \tag{20}$$

and

$$N = N_{pi} + N_{pr}, \qquad n_{pi} = N_{pi}/N, \qquad n_{pr} = 1 - n_{pi}, \tag{21}$$

where N_{pi} is the number of incoming particles per volume arriving in the control volume and N_{pr} the number of reflected particles per volume leaving the control volume. From Eqs. 19a and 20 we obtain

$$n_{pi}/n_{pr} = \bar{e}_p^N \tag{22}$$

and with Eq. 21 we have

$$\bar{e}_p^N = n_{pi}/(1 - n_{pi}) \qquad \text{and} \qquad n_{pi} = \bar{e}_p^N/\left(1 + \bar{e}_p^N\right). \tag{23}$$

We connect Eulerian quantities with Lagrangian quantities at the top of the control volume

$$\left(N \mid \overline{W}_{p,h}^{N,E} \mid A_n\right)\left(\overline{W}_{p,h}^{N,E}\right)^q = \left(N_{pi} \mid \overline{W}_{pi,h}^{N,L} \mid A_n\right)\left(\overline{W}_{pi,H}^{N,L}\right)^q + \left(N_{pr} \mid \overline{W}_{pr,h}^{N,L} \mid A_n\right)\left(\overline{W}_{pr,h}^{N,L}\right)^q \tag{24a}$$

or

$$\left(\overline{W}_{p,h}^{N,E}\right)^{q+1} = \left(\overline{W}_{pi,h}^{N,L}\right)^{q+1} n_{pi}\left[1 + (n_{pr}/n_{pi})\left(\bar{e}_p^N\right)\left(-\bar{e}_p^N\right)^q\right], \tag{24b}$$

where the superscript E denotes the Eulerian average quantity, and since $\mid \overline{W}_{pr,h}^{N,L} \mid \le \mid \overline{W}_{pi,h}^{N,L} \mid$ when $\bar{e}_p^N \le 1$, $\overline{W}_{p,h}^{N,E}$ is in same direction with $\overline{W}_{pi,h}^{N,L}$. From Eq. 24b with Eqs. 22 and 23, it follows that

$$\overline{W}_{p,h}^{N,E} = \overline{W}_{pi,h}^{N,L} B^N \qquad \text{and}$$

$$B^N = \left\{ \frac{\bar{e}_p^N\left[1.0 + \left(-\bar{e}_p^N\right)^q\right]}{1.0 + \bar{e}_p^N} \right\}^{1/(q+1)}, \tag{25}$$

where q is a factor required for the averaging process, $1 \le q \le 2$; $q = 1$ refers to a momentum average and $q = 2$ corresponds to an energy average. An equivalent formula to Eq. 24a applies to the tangential component of velocity and, using Eqs. 19b, 22, and 23, one obtains

$$\overline{W}_{p,h}^{T,E} = \overline{W}_{pi,h}^{T,L} B^T \qquad \text{and} \qquad B^T = \left\{ \frac{\bar{e}_p^N + \left(\bar{e}_p^T\right)^{q+1}}{1.0 + \bar{e}_p^N} \right\}^{1/(q+1)}. \tag{26}$$

By analogy to the flow of gas molecules, the normal and tangential Eulerian velocities of the particulate phase at $\eta = h$ from the wall can be linked to the Eulerian solution at $\eta = 0$, using a Taylor's expansion (Kogan, 1969)

$$\overline{W}_{p,h}^{N,E} \approx \overline{W}_{p,w}^{N,E} + h\left[\frac{\partial \overline{W}_p^{N,E}}{\partial \eta}\right]_w \qquad \text{and}$$

$$\overline{W}_{p,h}^{T,E} \approx \overline{W}_{p,w}^{T,E} + h\left[\frac{\partial \overline{W}_p^{T,E}}{\partial \eta}\right]_w. \tag{27}$$

At the wall we can use the equivalent of Eq. 24a to link the Eulerian and Lagrangian solution, except that $n_{pi} = n_{pr} = 0.5$ for steady flow,

$$\overline{W}_{p,w}^{N,E} = \overline{W}_{pi,w}^{N,L} A^N \quad \text{and} \quad A^N = \left[\frac{1.0 + \bar{e}_p^N \left(-\bar{e}_p^N \right)^q}{2} \right]^{1/(q+1)} \tag{28}$$

and

$$\overline{W}_{p,w}^{T,E} = \overline{W}_{pi,w}^{T,L} A^T \quad \text{and} \quad A^T = \left[\frac{1.0 + \left(\bar{e}_p^T \right)^{q+1}}{2} \right]^{1/(q+1)} \tag{29}$$

We need to link the Lagrangian solution at $\eta = h$ with Lagrangian solution at $\eta = 0$ and assume:

$$\overline{W}_{pi,h}^{N,L} \approx \overline{W}_{pi,w}^{N,L} \quad \text{and} \quad \overline{W}_{pi,h}^{T,L} \approx \overline{W}_{pi,w}^{T,L}. \tag{30}$$

As we can see, Eq. 30 is a good approximation for high inertia particles. For low inertia particles, we can introduce a local Knudsen number Kn, which is defined by a gas–particle interaction length, l_{gp}, divided by the system characteristic length, D, to connect to the change due to the aerodynamic drag between $\eta = 0$ and $\eta = h$. For turbulent flow, $l_{gp} = t_p |W_R'|$ as defined in Soo (1984), where $|W_R'|$ is the modulus of the relative turbulence intensity. In the present work we take the slip velocity $|W_R|$ instead of the relative turbulence. We use $Kn_h = h(l_{gp}/D) = hKn$ to replace h in Eq. 27 (where $Kn_h < h$, that is, when Kn is larger than one, we impose $Kn = 1$ because we only adjust for low inertia particles). Combining equations from Eqs. 25 to 30, one obtains

$$(A^N - B^N)\overline{W}_{p,w}^{N,E} + A^N Kn_h \left[\frac{\partial \overline{W}_p^{N,E}}{\partial \eta} \right]_w = 0 \tag{31}$$

and

$$(A^T - B^T)\overline{W}_{p,w}^{T,E} + A^T Kn_h \left[\frac{\partial \overline{W}_p^{T,E}}{\partial \eta} \right]_w = 0. \tag{32}$$

The condition of zero mass flux at the wall may be written as

$$\left[\frac{\partial \left(\rho_p \overline{W}_p^{N,E} \right)}{\partial \eta} \right]_w = \rho_{p,w} \left[\frac{\partial \left(\overline{W}_p^{N,E} \right)}{\partial \eta} \right]_w + \overline{W}_p^{N,E} \left[\frac{\partial (\rho_p)}{\partial \eta} \right]_w = 0. \tag{33}$$

From the Eqs. 33 and 31, we have

$$(B^N - A^N)\rho_{p,w} + A^N Kn_h \left[\frac{\partial \rho_p}{\partial \eta} \right]_w = 0. \tag{34}$$

Thus, the generalized wall boundary conditions for the particulate phase can be written in a generic form

$$a\varphi_w + b \left[\frac{\partial \varphi}{\partial \eta} \right]_w = c, \qquad \varphi = \left[W_p^N, W_p^T, \rho_p \right], \tag{35}$$

where $\overline{W}_p^{N,E}$ and $\overline{W}_p^{T,E}$ are replaced by W_p^N and W_p^T, and the coefficients in the equation can be obtained by

$$\begin{aligned} a_N &= A^N - B^N; & b_N &= A^N Kn_h; & c_N &= 0 \\ a_T &= A^T - B^T; & b_T &= A^T Kn_h; & c_T &= 0 \\ a_\rho &= B^N - A^N; & b_\rho &= A^N Kn_h; & c_\rho &= 0. \end{aligned} \tag{36}$$

Numerical Procedure

A versatile nonorthogonal boundary-fitted coordinate grid system is employed. The grids illustrated in Figure 2 are $22 \times 102 \times 12$ in the radial, axial, and spanwise direction, respectively, where a symmetry condition is imposed in the spanwise direction. The 45 control volumes in streamwise direction (that is, 2 degrees each) are used for the 90° bend. The distance of top surface of the first control volume adjacent to the wall, h, varies between 10 mm (for coarse grids) and 1.5 mm (for fine or stretching grids) in the present study.

Equation 1 is discretized using a finite volume formulation in generalized coordinate space, with the metric information expressed in terms of area vectors. The equations are solved on a nonstaggered grid, that is, all primitive variables are stored at the centroids of the mass control volumes. The velocity components in fixed Cartesian directions are treated as scalars after the transformation from physical coordinates to computational space coordinates. To approximate the convective terms at faces of the control volumes, a generalized QUICK convective differencing method (Cho et al., 1991) is used. Second derivatives are evaluated using three-point symmetric formulas. Each governing equation is sequentially relaxed to update one of the primitive variables. A velocity potential correction (Fletcher and Bain, 1991) is introduced to satisfy continuity of gas phase and upgrade the gas pressure using a modified SIMPLEC algorithm (Van Doormaal and Raithby, 1984). The stored values at the centroids are interpolated and modified to calculate the flow flux at faces of the control volumes using the moment interpolation method (Rhie and Chow, 1983). The governing equations for both the gas and particulate phase are solved sequentially at each iteration to obtain all the dependent variables. At each global iteration each equation is iterated, typically 3 to 5 times, using a strongly implicit procedure (Fletcher, 1991) scheme.

Results and Comparisons

In this article, we have focused our attention on comparisons of mean quantities of both the gas and particulate phases, specially the mean particulate velocities and concentration distribution in the bend, because the mean quantities are of more interest in engineering applications. All comparisons presented in this section are at the symmetry plane of the bend. The flow conditions used in the computations for

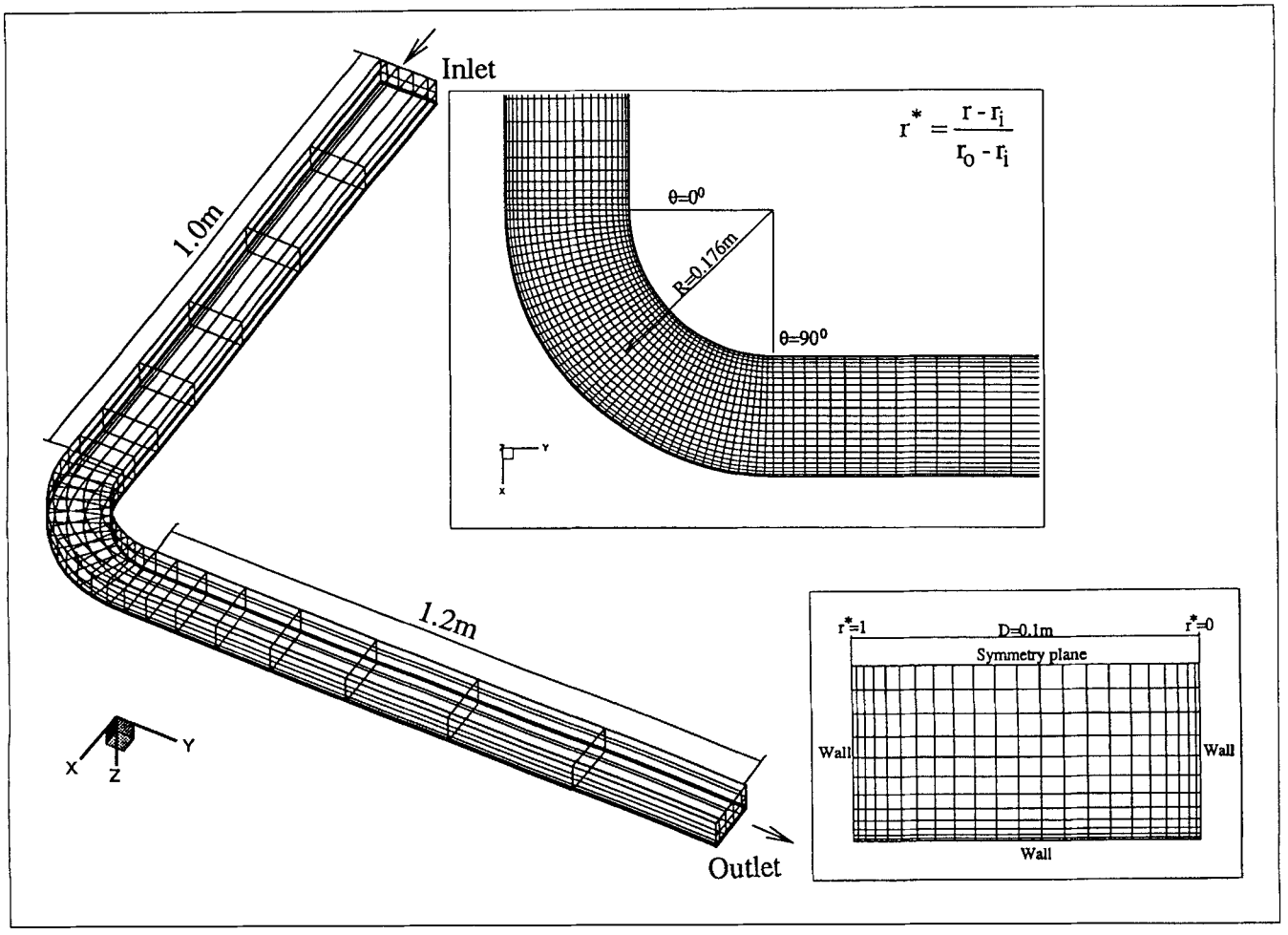

Figure 2. Computational domain and grids of a 90° square-sectioned bend.

the comparison with the experiment (except where indicated) are the bulk velocity (uniform velocity of both the gas and particulate phases at the top inlet 1 m away from the bend entrance as obtained by the experiment) is $U_b = 52.19$ m/s corresponding to the Reynolds number 3.47×10^5; the inlet turbulence intensity of the gas phase is 1%; the particle diameter size is 50 μm; the particle material density $\rho_s = 2{,}990$ kg/m^3; the inlet particulate bulk density $\rho_{p,in} = 1.8 \times 10^{-4}$ kg/m^3. The corresponding particle loading and volumetric ratios are 1.5×10^{-4} and 6×10^{-8}, respectively, for which the particle suspension is very dilute.

The grid independent solutions (uniform grids are refined) of mean streamwise velocity profiles carried out for the single phase (the gas phase in the absence of solids) at the bend entrance and the $\theta = 15°$ and 30° stations are shown in Figure 3. It can be seen from this figure that the two finest grids have yielded almost identical solutions that are in very good agreement with Kliafas and Holt's measurements. The predictions of streamwise turbulence intensity using two different turbulence models, compared with the measurements, are presented in Figure 4. The high turbulence intensity near the two side walls is observed and the predictions of turbulence intensity using the standard k-ϵ turbulence model are higher than those using the RNG-based k-ϵ turbulence model. It is found that there exists an underprediction of turbulence intensity near the outer wall using the RNG-based k-ϵ turbulence model and an overprediction near the inner wall using the standard k-ϵ turbulence model.

In order to address whether the continuum assumption implicit in using a Eulerian model for the particulate phase is satisfactory since a very dilute particle suspension was used in Kliafas and Holt's experiment, a set of numerical computations are intentionally performed in this work.

In order to address whether the continuum assumption implicit in using a Eulerian model for the particulate phase is satisfactory since a very dilute particle suspension was used 12 in the radial, streamwise, and spanwise directions, respectively. The number of particles in a small control volume in this case will be of the order of 10^3. Figure 5 shows a numerical computation compared with the experimental data when using three sets of inlet condition of particulate concentration, where $\rho_{p,\text{in}} = 1.8 \times 10^{-4}$ kg/m^3 corresponds to the experimental condition. The numerical results are almost identical and in good agreement with the experimental data, except for some uncertainty about the experimental particulate concentration near the inner wall. As discussed in the experiments of Kliafas and Holt, the particle distribution is quite uniform at the bend entrance and, in moving downstream,

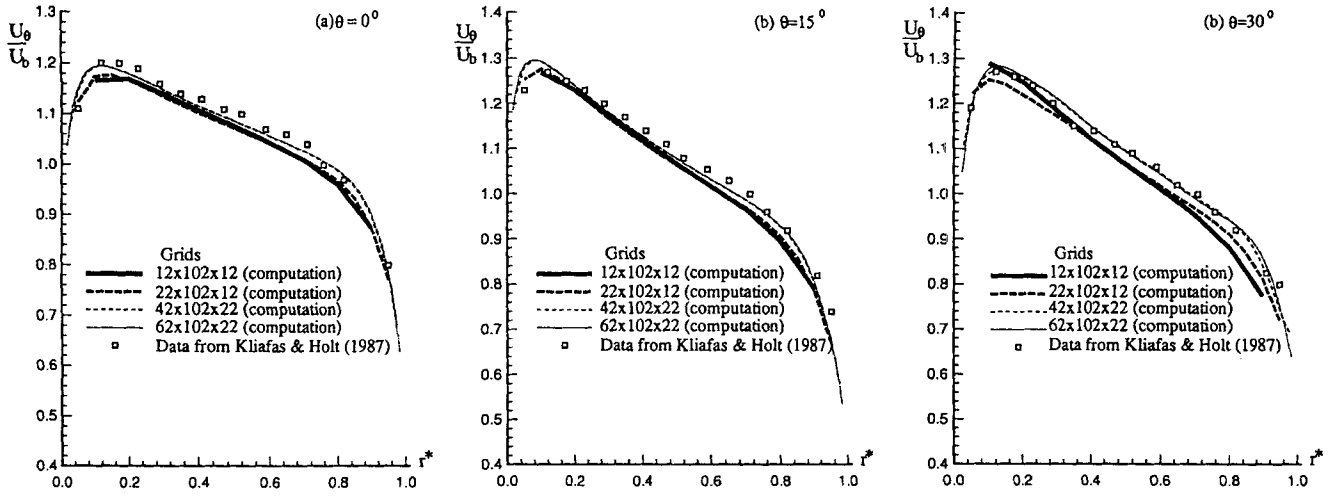

Figure 3. Grid independent solutions of the mean streamwise gas velocity profiles.

much higher particulate concentrations appear gradually nearer the outer wall than those near the inner wall. Thus, the occasional increase of particulate concentration near the inner wall at $\theta = 15°$ is not consistent with their discussions.

The particulate concentration from the computation is normalized by each inlet value and then by a reference value (dimensionless). The reference value is taken from the maximum value of the computational results and of the experimental data, respectively. By using this procedure, the particle distribution in a whole 90° bend from the computation can be compared with measured data.

Figure 6 shows the effect of grid refinement on the computational results of the particulate phase. In this case, a medium inlet particulate density $\rho_{p,in} = 0.018$ kg/m^3 (corresponding to a volumetric ratio 6×10^{-6}) is used, for which the control volumes in the finest grids cannot contain a sufficient number of particles. It is interesting that the numerical results, for both the grid refinement and the reduction of particulate loading (see Figure 5), do not show any sudden discontinuity or divergence from the case with sufficient particles in individual computational volumes to the case without sufficient particles. This observation suggests that we are not required so strictly to follow the continuum condition when using two-fluid models if the mean values of the particulate phase can be obtained by an experimental technique. In addition it is necessary that the range of solutions corresponding to the range of concentrations all lie within one flow regime. In the present case all the concentrations correspond to one-way coupling. The accuracy of numerical predictions using an Eulerian approach will depend on how the boundary conditions, particle–wall collisions, turbulent interactions, and other physical phenomena can be appropriately modeled.

Figure 7 shows comparisons of predicted mean streamwise velocity profiles of both the gas and particulate phase with measured data, at $\theta = 0°$, 15°, and 30° stations, respectively. The large negative slip velocity between the gas and particulate flow appears near the outer wall. The maximum values of gas velocity profiles is displaced toward the inner wall, as a result of the favorable streamwise pressure gradient present there (see Figure 8). In Figure 8, the pressure coefficient is calculated by $C_p = (P - P_{in})/(0.5\rho_g U_b^2)$, where P_{in} is the in-

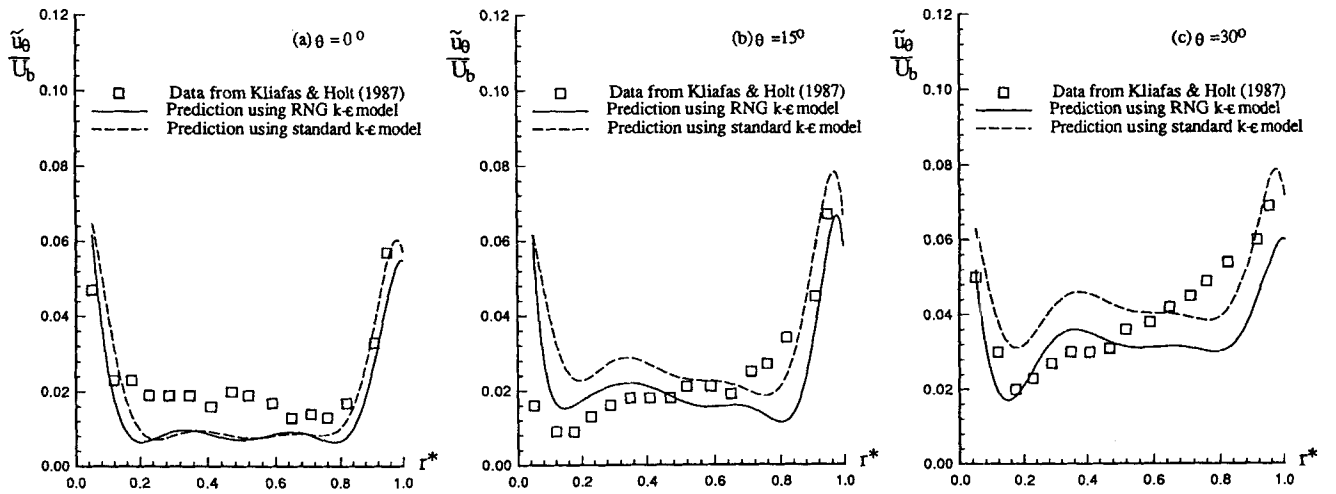

Figure 4. Measurements and calculations of streamwise turbulence intensity profiles.

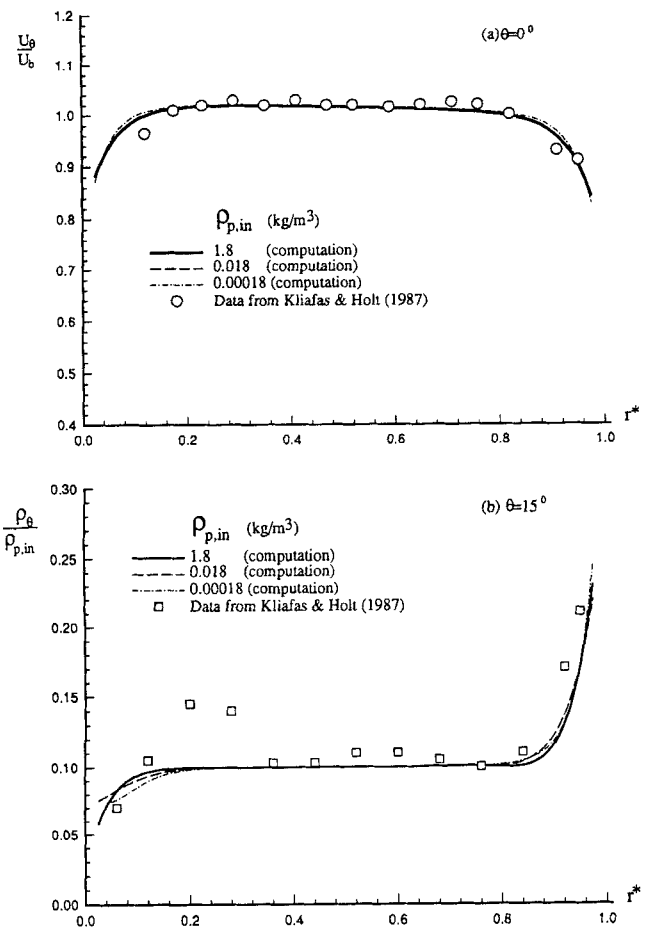

Figure 5. (a) Mean streamwise particulate velocity at bend entrance; (b) particulate concentration distribution at $\theta = 15°$ station, as a function of three different inlet conditions of particulate concentration.

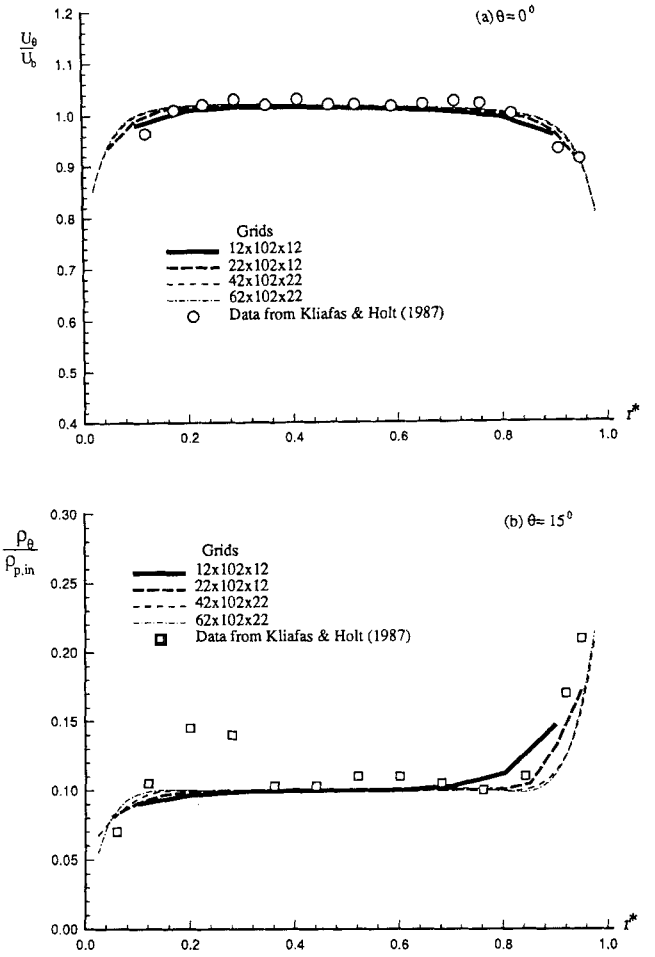

Figure 6. Effect of grid refinements on (a) mean streamwise velocity and (b) concentration.

let gas pressure. It is also found from Figure 7 that there is deceleration of the flow near the outer wall due to the unfavorable pressure gradient on the upper half of the bend.

It can be see from Figure 7 that the particulate velocity profiles at all stations are relatively flat. It can be concluded from these results that the particulate velocity profiles are not affected by the gas pressure gradient that caused the dis-

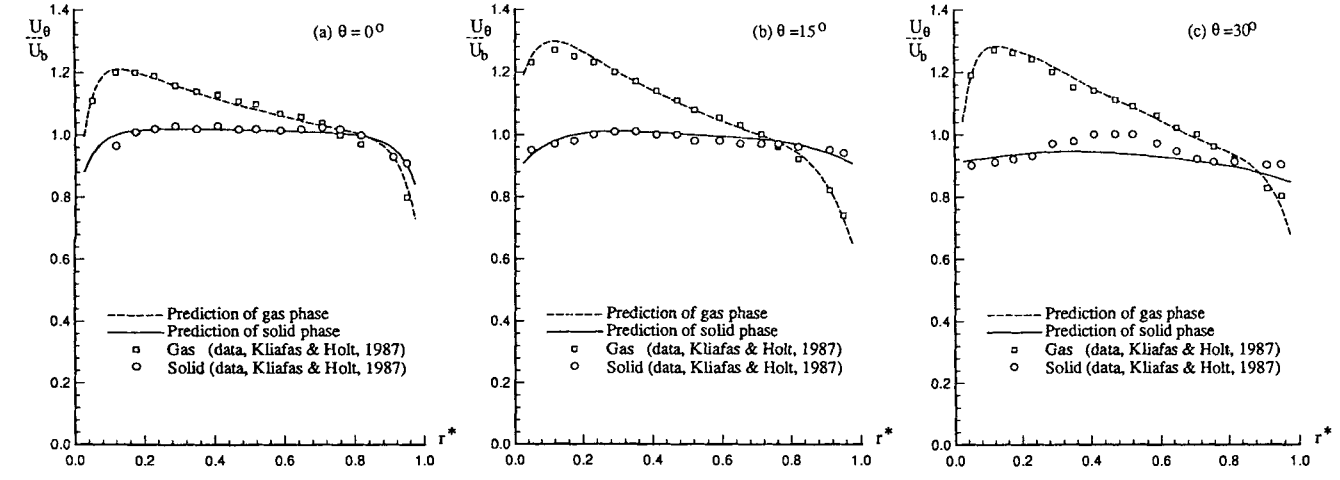

Figure 7. Comparisons of predicted mean streamwise velocity profiles of both gas and particulate phases with measured data.

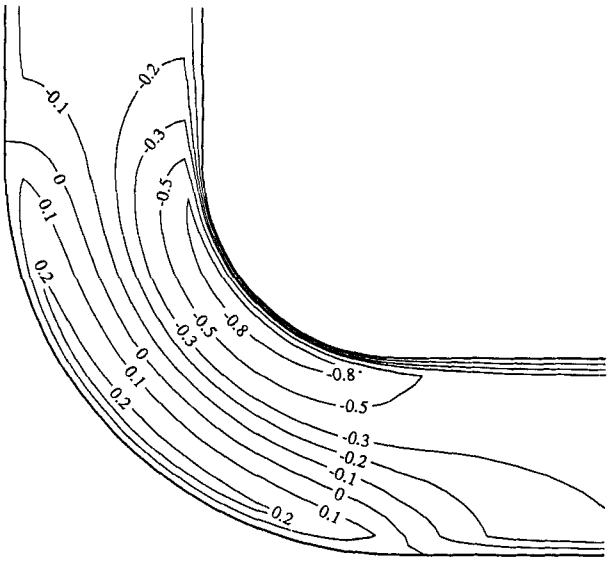

Figure 8. Distribution of pressure coefficient of gas phase flow in the bend.

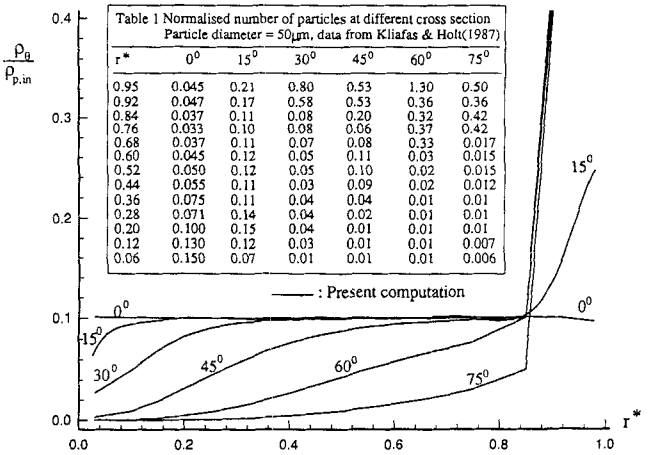

Figure 10. Comparison of normalized particulate concentration between the prediction and measurement at different stations along the symmetry plane of the bend.

placement of the maximum gas velocities toward the inner wall. The current numerical model has yielded very satisfactory results for the prediction of mean streamwise velocity profiles of both the gas and particulate phases.

Figure 9 shows a numerical prediction of gas–particle flow through the 90° bend in terms of velocity vectors and normalized concentration distribution at the symmetry plane. It can be seen from Figure 9a that particles follow the gas flow into the bend entrance and then, due to their own inertia, collide with the outer wall directly. It can be seen from Figure 9b that very few particles are found in the region near the inner wall of the bend. It can be concluded that particle–wall interaction is a main controlling factor for the outer wall region of the flow. This is also in agreement with the observation by Kliafas and Holt that only the outer wall was impacted by particles and the inner wall was, in general, erosion free in their experiment.

A remarkable qualitative agreement of the predicted concentration distribution with the measured data can be found from Figures 9b and 10. The discussions about particle distribution according to the observation by Kliafas and Holt can generally be repeated for the present numerical prediction. The particle distribution upstream of the bend entrance is found to be quite uniform. From the station $\theta = 15°$, a much higher particle concentration appears near the outer wall than

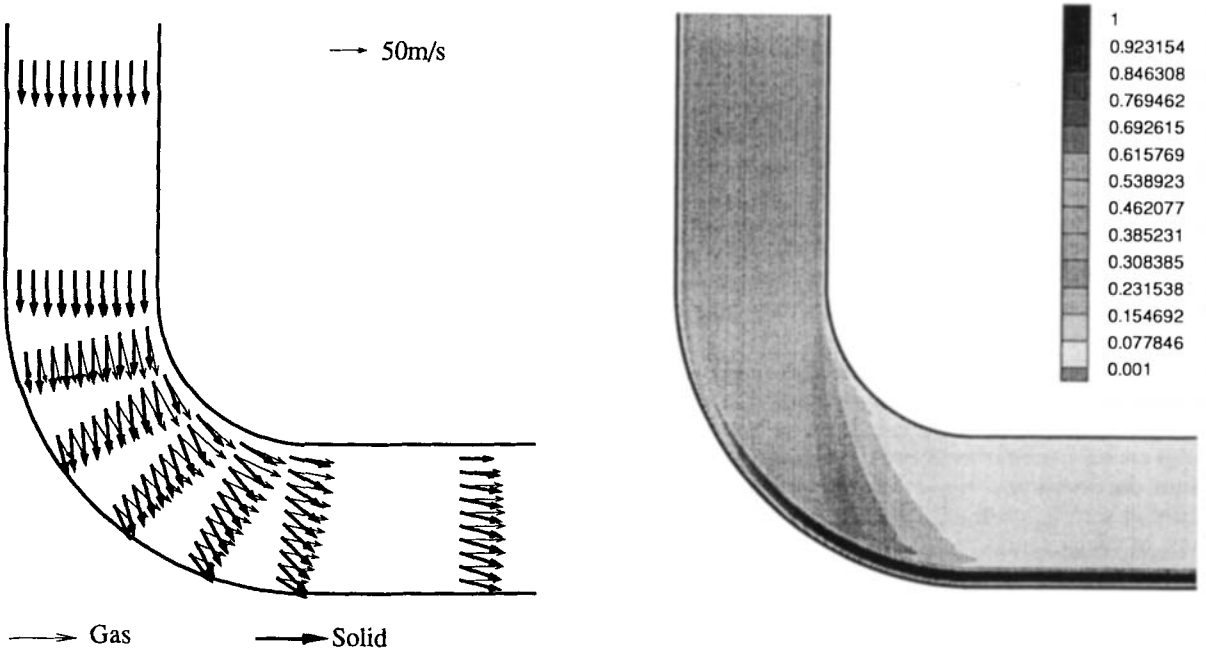

Figure 9. Numerical predictions of gas-solid particle flow in a 90° bend in terms of (a) velocity vectors of both gas and particulate phases, and (b) normalized particulate concentration distribution.

near the inner wall. The particle concentration is further increased near the outer wall and further decreased near the inner wall with the increase of the turning of the bend. From the middle station of the bend, a particle-free region starts to be identified close to the inner wall. The thickness of this particle-free region gradually increases until the bend exit. This large particle-free area extends almost from the bend exit fully downstream. This behavior is attributed by Kliafas and Holt to the high gas bulk velocities employed in the study.

Finally, it is interesting to point out that for the present case, both from the measurements and computations, it is found that the influence of the turbulence on the mean particulate flow is very small due to the high inertia of solid particles. When two different flow conditions (two different bulk velocities and turbulence intensities) were employed in the experiment, it yielded almost identical mean streamwise velocity profiles for the particulate phase. When using two different turbulence models in the computation, the prediction of turbulence intensity using a standard k-ϵ turbulence model is higher than when using a RNG-based k-ϵ turbulence model, but the mean streamwise velocity profiles of the particulate phase are almost not changed. As has been pointed out by Kliafas and Holt, among the many factors that may influence the behavior of the particulate flow, the particle–wall interaction proves to be a controlling factor in the present study.

Conclusions

Numerical computations and comparisons with the LDV results of Kliafas and Holt (1987) for turbulent gas–solid particle flow in a 90° square-sectioned bend are reported in this article. A Eulerian model, including generalized wall-boundary conditions for the particulate phase and a particle–wall collision model, is employed. The comparison of the mean streamwise velocity profiles of both the gas and particulate phases gives very satisfactory agreement with the Kliafas and Holt's data. For the distribution of the particulate concentration, a remarkable qualitative agreement of the prediction with the measured data is demonstrated in the present work.

There may be many factors that influence the behavior of solid particles in turbulent two-phase flows, such as viscous shear due to the presence of the wall, fluid/turbulence interaction, particle–particle and particle–wall interactions, deposition of particles on the duct wall, just to name a few. Of these, from both computational and experimental studies, particle–wall interaction proves to be the controlling factor in the present case.

The direct application of the present study would be to the development of large coal gasification plants. The detailed numerical computation of two-phase flows in curved ducts would also enable material scientists and engineers to predict and study parametrically the erosion characteristics and mechanism in such geometries, and subsequently to improve the design of components.

Acknowledgment

The authors are grateful to DIST and Pacific Power (Electricity Commission of New South Wales, Australia) for the financial support provided as part of the DS4PUB project.

Notation

a,b,c = coefficients in boundary equations, Eq. 36
A^N, A^T = coefficients in boundary equations, Eqs. 25–26
C_μ = turbulence model constant equal to 0.0837
$C_{\epsilon 1}$ = turbulence model constant equal to 1.42
$C_{\epsilon 2}$ = turbulence model constant equal to 1.68
D = hydraulic diameter (100 mm)
k = turbulent kinetic energy
K_d = weight factors equal to 0.01
n = fraction of particle number
P_k = turbulence production
r^* = normalized radial coordinate, $r^* = (r - r_i)/(r_o - r_i)$
r_i = radius of curvature of the inner wall
r_o = radius of curvature of the outer wall
Re = Reynolds number, $Re = (U_b D)/\nu$
u,v,W = mean velocity
u',v',W' = fluctuating velocity
$\tilde{u}_\theta/U_b$ = streamwise turbulence intensity
U_θ = mean streamwise velocity
x = Cartesian coordinate
y^+ = dimensionless distance from solid wall

Greek letters

ϵ = dissipation of turbulent kinetic energy
κ = von Karman constant equal to 0.41
μ = viscous coefficient
η = normal direction in general coordinates
ρ_g = bulk density of gas phase

Subscripts and superscripts

i,j = 1,2,3 (u,v,w)
g = gas phase
N = normal direction
p = particulate phase
T = tangent direction
w = wall
i,j = 1, 2, 3 (x, y, z)
L = Lagrangian quantity

Literature Cited

Adeniji-Fashola, A., and C. P. Chen, "Modelling of Confined Turbulent Fluid-Particle Flows Using Eulerian and Lagrangian Schemes," *Int. J. Heat Mass Transf.*, **33**, 691 (1990).

Chen, C. P., and P. E. Wood, "A Turbulence Closure Model for Dilute Gas-Particle Flows," *Can. J. Chem. Eng.*, **63**, 349 (1985).

Chen, C. P., and P. E. Wood, "Turbulence Closure Model of the Dilute Gas-Particle Axisymmetric Jet," *AIChE J.*, **32**, 163 (1986).

Cho, N-H., C. A. J. Fletcher, and K. Srinivas, "Efficient Computation of Wing Body Flows," *Lecture Notes in Physics*, **371**, Springer-Verlag, New York, p. 167 (1991).

Elghobashi, S., "On Predicting Particle-Laden Turbulent Flows," *Appl. Sci. Res.*, **52**, 309 (1994).

Fletcher, C. A. J., *Computational Techniques for Fluid Dynamics: 1. Fundamental and General Techniques; 2. Specific Techniques for Different Flow Categories*, 2nd ed., Springer-Verlag, Heidelberg (1991).

Fletcher, C. A. J., "Gas Particle Industrial Flow Simulation Using RANSTAD," *Surveys in Fluid Mechanics*, R. Narasimha, ed., Indian Academy of Science, **18**, Parts 3 and 4, 657 (1993).

Fletcher, C. A. J., and J. G. Bain, "An Approximate Factorisation Explicit Method for CFD," *Comput. Fluids*, **19**, 61 (1991).

Gosman, A. D., et al., "Multidimensional Modeling of Turbulent Two-Phase Flows in Stirred Vessels," *AIChE J.*, **38** (12), 1946 (1992).

Ilias, S., and P. L. Douglas, "Inertial Impaction of Aerosol Particles on Cylinders at Intermediate and High Reynolds Numbers," *Chem. Eng. Sci.*, **44**, 81 (1989).

Issa, R., and P. J. Oliveira, "Numerical Prediction of Phase Separation in Two-Phase Flow Through T-Junctions," *Comput. Fluids*, **23**(2), 347 (1994).

Kliafas, Y., and M. Holt, "LDV Measurements of a Turbulent Air-Solid Two-Phase Flow in a 90° Bend," *Exp. Fluids*, **5**, 73 (1987).

Kogan, M. N., *Rarefied Gas Dynamics*, Plenum Press, New York (1969).
Launder, B. E., and D. B. Spalding, "The Numerical Computation of Turbulent Flows," *Comp. Methods Appl. Mech. Eng.*, **3**, 269 (1974).
Pourahmadi, F., and J. A. C. Humphrey, "Modeling Solid-Fluid Turbulent Flows with Application to Predicting Erosive Wear," *Int. J. Phys. Chem. Hydro Dynam.*, **4**, 191 (1983).
Reeks, M. W., "On the Continuum Equations for Dispersed Particles in Nonuniform Flows," *Phys. Fluids*, **A4**, 1290 (1992).
Reeks, M. W., "On the Constitutive Relations for Dispersed Particles in Nonuniform Flows: 1. Dispersion in a Simple Shear Flow," *Phys. Fluids*, **A5**, 750 (1993).
Rhie, C. M., and W. L. Chow, "Numerical Study of the Turbulent Flow Past an Airfoil with Trailing Edge Separation," *AIAA J.*, **21**, 1525 (1983).
Rizk, M., and S. E. Elghobashi, "A Two-Equation Turbulence Model for Dispersed Dilute Confined Two-phase Flows," *Int. J. Multiphase Flow*, **15**, 119 (1989).
Schuh, M. J., C. A. Schuler, and J. A. C. Humphrey, "Numerical Calculation of Particle-Laden Gas Flows Past Tubes," *AIChE J.*, **35**, 466 (1989).
Simonin, O., E. Deutsch, and M. Boivin, "Large Eddy Simulation and Second-Moment Closure Model of Particle Fluctuating Motion in Two-Phase Turbulent Shear Flows," *Proc. 9th Symp. on Turbulent Shear Flows*, F. Durst et al., eds., Springer-Verlag, Berlin (1994).
Sommerfeld, M., "Modelling of Particle-Wall Collisions in Confined Gas-Particle Flows," *Int. J. Multiphase Flow*, **18**, 905 (1992).
Soo, S. L., "Development of Theories on Liquid Solid Flows," *J. Pipeline*, **4**, 137 (1984).
Tu, J. Y., and C. A. J. Fletcher, "Eulerian Modelling of Dilute Particle-Laden Gas Flows Past Tubes," DS4PUB Tech. Rep. 94-11, CANCES, University of New South Wales, Sydney, Australia (1994).
Van Doormaal, J. P., and G. D. Raithby, "Enhancements for the SIMPLE Method for Predicting Incompressible Fluid Flow," *Numer. Heat Trans.*, **7**, 147 (1984).

Manuscript received Apr. 18, 1994, and revision received Nov. 18, 1994.